Available online at www.sciencedirect.com
SCIENCE DIRECT®
Materials Chemistry and Physics 91 (2005) 1–9
MATERIALS CHEMISTRY AND PHYSICS
www.elsevier.com/locate/matchemphys

Structure of the Mg_2Ni switchable mirror: an EXAFS investigation

M. Di Vece[a,*], A.M.J. van der Eerden[b], D. Grandjean[b], R.J. Westerwaal[c], W. Lohstroh[c], S.G. Nikitenko[d], J.J. Kelly[a], D.C. Koningsberger[b]

[a] *Debye Institute, Condensed Matter and Interfaces, Utrecht University, P.O. Box 80000, 3508 TA Utrecht, The Netherlands*
[b] *Debye Institute, Inorganic Chemistry and Catalysis, Utrecht University, P.O. Box 80083, 3508 TA Utrecht, The Netherlands*
[c] *Faculty of Sciences, Division of Physics and Astronomy, Vrije Universiteit De Boelelaan 1081, 1081 HV Amsterdam, The Netherlands*
[d] *DUBBLE CRG, ESRF, BP 220, 38043 Grenoble Cedex 9, France*

Received 11 July 2004; received in revised form 2 September 2004; accepted 9 September 2004

Abstract

Hydrogen intercalation changes both the structure and the optical properties of Mg_2Ni thin films. The structure of evaporated thin films was investigated in the as-deposited, hydrogenated and dehydrogenated states with extended X-ray absorption fine structure (EXAFS) and X-ray diffraction (XRD). The partially crystalline virgin film becomes completely amorphous upon hydrogenation. After removal of the intercalated hydrogen the film remains amorphous. Hydrogen was detected in different concentrations in the virgin, hydrogenated and dehydrogenated films. Hydrogen loading was confirmed both by a shift of the nickel absorption edge and an increase of the hydrogen content. The intercalated hydrogen in the completely loaded film is located around the nickel atom with a coordination close to four.

Keywords: Thin films; Optical materials; XAFS (EXAFS); Lattice dynamics; Crystal structure

1. Introduction

The term ‘switchable mirror’ refers to a range of metal and alloy thin films, which show striking optical properties upon hydrogenation [1]. A reflective thin metal film becomes transparent at a certain concentration of absorbed hydrogen. Soon after the discovery of the first switchable mirrors [2], yttrium and rare-earth metal thin films, magnesium was introduced as an alloying element [3]. The magnesium provides colour neutrality in the transparent state and gives an intermediate, optically highly absorbing state. A solid-state device based on a gadolinium–magnesium alloy has been fabricated [4]. Richardson et al. [5] have shown that magnesium can also be alloyed with the first-row transition metals to provide optical switching properties. Of these, Mg_2Ni is an interesting material [5] because of the general availability of the elements and the insensitivity of the alloy to oxidation, as compared to yttrium or the rare-earth metals. This alloy, well-known from hydrogen-storage research [6], has been studied extensively. Upon hydrogenation, the structure of Mg_2Ni remains unchanged up to the $Mg_2NiH_{0.3}$ composition [7]. For higher hydrogen concentrations, a structural rearrangement occurs until the fully loaded and transparent state (Mg_2NiH_4) is reached. However, before the transparent state, an optically highly absorbing state has been observed [8]. The structure of the low-temperature bulk Mg_2NiH_4 is known from X-ray diffraction (XRD) and neutron diffraction experiments. A distinction between the high and low-temperature phases (HT and LT, respectively) can be made [9]. Both have the CaF_2-type arrangement with $[NiH_4]^{4-}$ units surrounded by magnesium atoms at the corners of a cube. In contrast to the ordered HT phase, the LT phase is considerably distorted.

Calculations by Garcia et al. [10] indicated that the hydrogen configuration around the nickel atom has a

* Corresponding author. Present address: Nanoscale Physics Research Laboratory, School of Physics and Astronomy, The University of Birmingham, Birmingham B152TT, UK. Tel.: +44 121 414 4613; fax: +44 121 414 7327.
E-mail address: marcel@nprl.ph.bham.ac.uk (M. Di Vece).

0254-0584/$ – see front matter © 2004 Elsevier B.V. All rights reserved.
doi:10.1016/j.matchemphys.2004.09.008

significant effect on the band structure. Recent calculations by Myers et al. [11] also showed that the optical properties of cubic Mg_2NiH_4 are influenced by the hydrogen position in the NiH_4 complex in the alloy. However, XRD-amorphous thin films, which remain so upon complete hydrogenation and thus becoming transparent are reported by Farangis et al. [12]. The latter films are sputtered in contrast to the more common molecular beam epitaxy deposited switchable mirrors. However, this is not expected to influence the structure of the film. It raises the question as to whether a Mg_2NiH_4 film is completely amorphous or nanocrystalline since XRD cannot detect a lattice structure in very small crystallites. A structural model for the explanation of the optical properties can be applied to the structure of the nanocrystals. When the film is amorphous this is not possible.

Farangis et al. [12], recently studied the MgNi switchable mirror with X-ray absorption fine structure (XAFS) as a function of the magnesium–nickel ratio and following hydrogenation. They found an increase of disorder on alloying, as compared to the pure metals. Hydrogenation resulted in a positive shift of the absorption edge, indicating a charge transfer. However, they were not able to provide structural information on the hydrogenated film due to a low external X-ray absorption fine structure (EXAFS) signal on the Ni $L_{2,3}$ edges.

An earlier EXAFS study of our group [13] on the gadolinium–magnesium switchable mirror provided valuable information on the structure of the alloy. These results showed that EXAFS could be well-suited to determine the degree of short-range order and the extent of segregation in Mg_2Ni thin films. Besides the structural information from EXAFS, the XAFS absorption edge together with the intensity of the white-line area also provides electronic information.

In this work, we investigated the short-range order of the Mg_2Ni switchable mirror with EXAFS at the Ni K-edge in the virgin, hydrogenated and dehydrogenated states. The XRD spectra of both the virgin and hydrogenated films are also presented. The results are important for future research, which tries to explain the optical change (metal–insulator transition) upon hydrogen loading and unloading in terms of band-structure calculations based on crystal structure.

2. Experimental details

2.1. Sample preparation

Mg_2Ni polycrystalline layers were deposited on thin glass slides by co-evaporation at 10^{-9} mbar base pressure at deposition rates of 0.56 Å s^{-1} for magnesium and 0.13 Å s^{-1} for nickel. Rutherford backscattering spectrometry showed a composition ratio of Mg:Ni = 1.73. The 14% deviation of Mg_2Ni is not expected to influence our results much. The films were nominally 300 nm thick and had a 3 nm cap-layer of palladium. The palladium serves as a catalyst for hydrogen dissociation and protects the film against oxidation.

2.2. Data collection

The XAFS spectra at the Ni K-edge were measured at the European Synchrotron Radiation Facility (Grenoble, France, DUBBLE beam-line), which was equipped with a Si (3 1 1) double-crystal monochromator. All measurements were performed in a standard cell [14] in the fluorescence mode, using a C-TRAIN detector with XSPRESS processing electronics [15]. The measurements were carried out on the as-deposited, fully hydrogenated and dehydrogenated films. Loading of the samples to the fully hydrogenated state was achieved by applying a hydrogen/helium flush at room temperature. Dehydrogenation was achieved by heating the film to 100 °C in ambient atmosphere. The spectra were measured at liquid nitrogen temperature.

2.3. Data analysis

The XDAP program developed by Vaarkamp et al. [16] was used for data analysis. Nine simultaneously recorded scans were averaged during data reduction. The pre-edge background was approximated by a modified Victoreen function before subtraction [17]. The edge energy was determined at the maximum of the first derivative of the spectrum. The spectrum was background corrected with a cubic spline routine [18]. Normalization was performed by dividing the absorption spectrum by the height of the background at 50 eV from the edge.

Ni–Ni, Ni–Mg, Ni–O and Ni–H references used for the fitting procedure were calculated with FEFF8 [19]. A Hedin–Linquist potential [20] was used to calculate the phase shift and the back-scattering amplitude. The value of the amplitude reduction factor (S_0^2) was calculated from the EXAFS data of a nickel foil, and used in the Mg_2Ni analysis. The crystallographic data and input parameters for FEFF8 used to create the EXAFS references are listed in Table 1.

The experimental data were fitted in the *R*-space by the difference file technique, which was applied to resolve the different contributions in the EXAFS data [21]. The EXAFS data-analysis program XDAP allows multiple-shell fitting in the *R*-space by minimizing the residuals between both the absolute and the imaginary part of the Fourier transforms (FT) of the data and the fit. The *R*-space fitting has important advantages compared to the usual fitting in the *k*-space and is extensively discussed in a recent paper by Koningsberger et al. [21]. More information about this method applied to

Table 1
Crystallographic data and input parameters for FEFF used to create the reference files

Absorber–backscatterer	*N*	*R* (Å)	S_0^2	V_r (eV)	V_i (eV)
Ni–Ni	1	3.00/4.20	0.8	0	0
Ni–Mg	1	2.65/4.00	0.8	0	0
Ni–H	1	1.55	1	0	0

S_0^2 is a amplitude reduction factor; V_r and V_i are the real and imaginary part of a potential correction.

a similar system can be found in a gadolinium–magnesium EXAFS study [13].

2.4. X-ray diffraction

X-ray diffraction experiments were performed with a Bruker B8 Discover diffractometer (Cu Kα: wavelength λ = 1.5418 Å) using a 2θ–θ geometry. A loading cell allowed the study of hydrogenation in situ, for pressures up to 1 bar of hydrogen. Unloading was carried out at 100 °C in air.

3. Results

The X-ray absorption K-edge spectra of the Mg_2Ni film in the as-deposited, hydrogenated and dehydrogenated states are shown in Fig. 1. Upon exposure of the film to hydrogen, the edge shifts from 2.7 eV to higher energy, while the heat treatment at 100 °C in air causes a shift back to lower energy, clearly confirming dehydrogenation. A shift of the absorption edge is usually the result of charge transfer from or to the probed atom. The X-ray absorption near-edge structure (XANES) changes slightly after each treatment.

Fig. 2a shows the raw EXAFS data for the virgin sample (solid line), the hydrogenated film (dotted line) and the dehydrogenated film (dashed line). The decrease of the amplitude of the wiggles in the EXAFS indicates a significant change of the coordination around nickel. A decrease of the EXAFS amplitude upon hydrogenation is clearly visible. The heat treatment, however, does not change the amplitude much, indicating only a minor change in the structure.

The k^1 weighed Fourier-transformed spectra of the raw EXAFS data are shown in Fig. 2b. The three Fourier transforms have a clear peak at about 2.4 Å. The decrease in amplitude of the main peak upon hydrogenation is evident. Dehydrogenation does not significantly change the amplitude of the Fourier transform of the hydrogenated film, again indicating only minor changes in the structure.

The EXAFS data could be effectively fitted with the scatterers magnesium, hydrogen and nickel. An oxygen contribution could not be detected, which shows that the film is

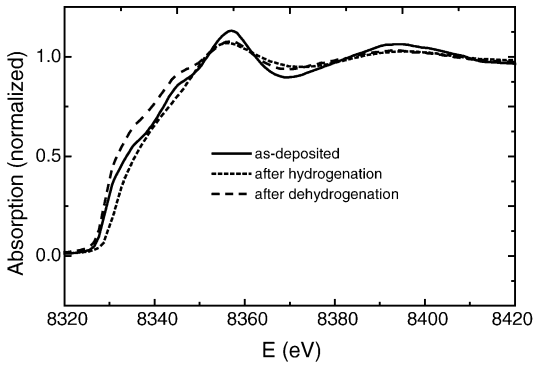

Fig. 1. The X-ray absorption K-edge spectra for the Mg_2Ni thin films.

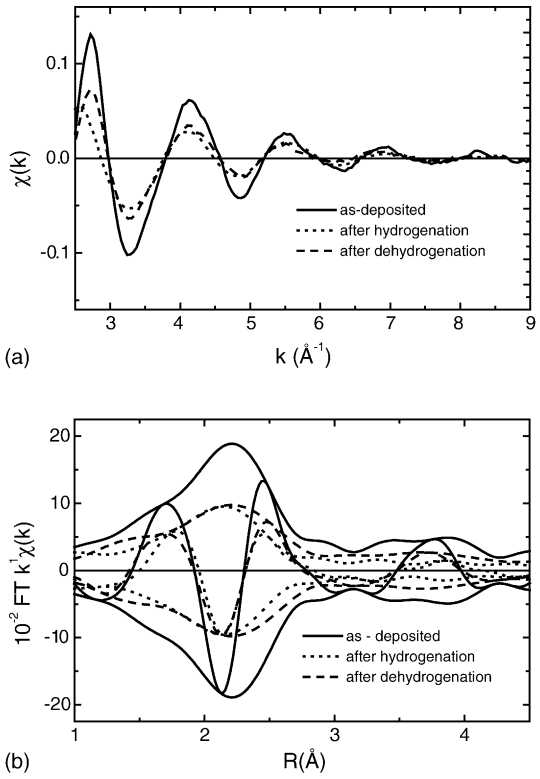

Fig. 2. (a) The EXAFS data after normalization and (b) the Fourier transform (k^1, Δk = 2.5–9 (8) $Å^{-1}$) for the Mg_2Ni films.

either insensitive to oxidation or the introduced oxygen is too disordered to be detected. The coordination number N and interatomic distances R pertaining to the nickel atom in the virgin film is shown in Table 2. A Ni–Mg contribution is detected in two shells at distances of 2.67 and 4.46 Å with a coordination of 5.3 and 7.2, respectively. Only a small Ni–Ni contribution is detected (N = 0.3) at a distance of 3.49 Å. Hydrogen is present in the virgin film as is clear from its coordination of 7.5 at a distance of 1.84 Å. This surprisingly high coordination will be explained in the following section. The presence of hydrogen is not unusual as shown by Di Vece et al. [13], since hydrogen may be present during the deposition of the film in the vacuum chamber.

The k^1 weighed FT of the raw EXAFS data (solid line) of the hydrogenated film is shown in Fig. 3a, together with the FT of the fit (dotted line). The fit matches the experimental data very well in the entire range of the analysis (1 Å < R < 4.5 Å). Clearly no other contributions are necessary to fit the raw EXAFS data accurately. As the high quality of this fit is representative for the fits of the virgin and dehydrogenated films, the latter are not shown.

The highest maximum in the absolute part of the FT of Fig. 3a is located at 2.4 Å. At larger distances more local maxima are present. The individual contributions to the FT fit, as-extracted with the difference file technique, are plotted in Fig. 3b–e. The difference file (solid line) of Fig. 3b could be well-described by the calculated Ni–Mg EXAFS (dotted

Table 2
Ni K-edge; sample Mg_2Ni/Pd as-synthesised; EXAFS analysis (2.5 Å^{-1} < k < 9 Å^{-1}) k^1-weighing

Absorber–backscatterer	N	R (Å)	$\Delta\sigma^2$ ($\times 10^{-3}$ Å^2)	ΔE_0 (eV)	k variance	
					Imaginary	Real
Ni–Mg	5.3	2.67	8.7	−8.08	0.43	0.25
Ni–H	7.3	1.84	17	7.87		
Ni–Mg	7.2	4.46	22	1.97		
Ni–Ni	0.3	3.49	0.8	0.3		

line) at 2.63 Å. Two Ni–H contributions have been detected as shown in Fig. 3c and d. The difference files (solid lines) are well fitted by the calculated Ni–H EXAFS (dotted line). The Ni–H contributions have peaks at about 1.25 and 1.4 Å. From the imaginary part of the FT it is clear that the two Ni–H shells have opposite phases. The FT of the difference file and calculated EXAFS of Ni–Ni are shown in Fig. 3e. The agreement between the FT of the difference file and the Ni–Ni EXAFS is of somewhat lower quality due to the influence of noise, since the amplitude of the FT is an order of magnitude lower than that of the other contributions. It is not clear if the differences at about 4 Å are due to a real contribution or a part

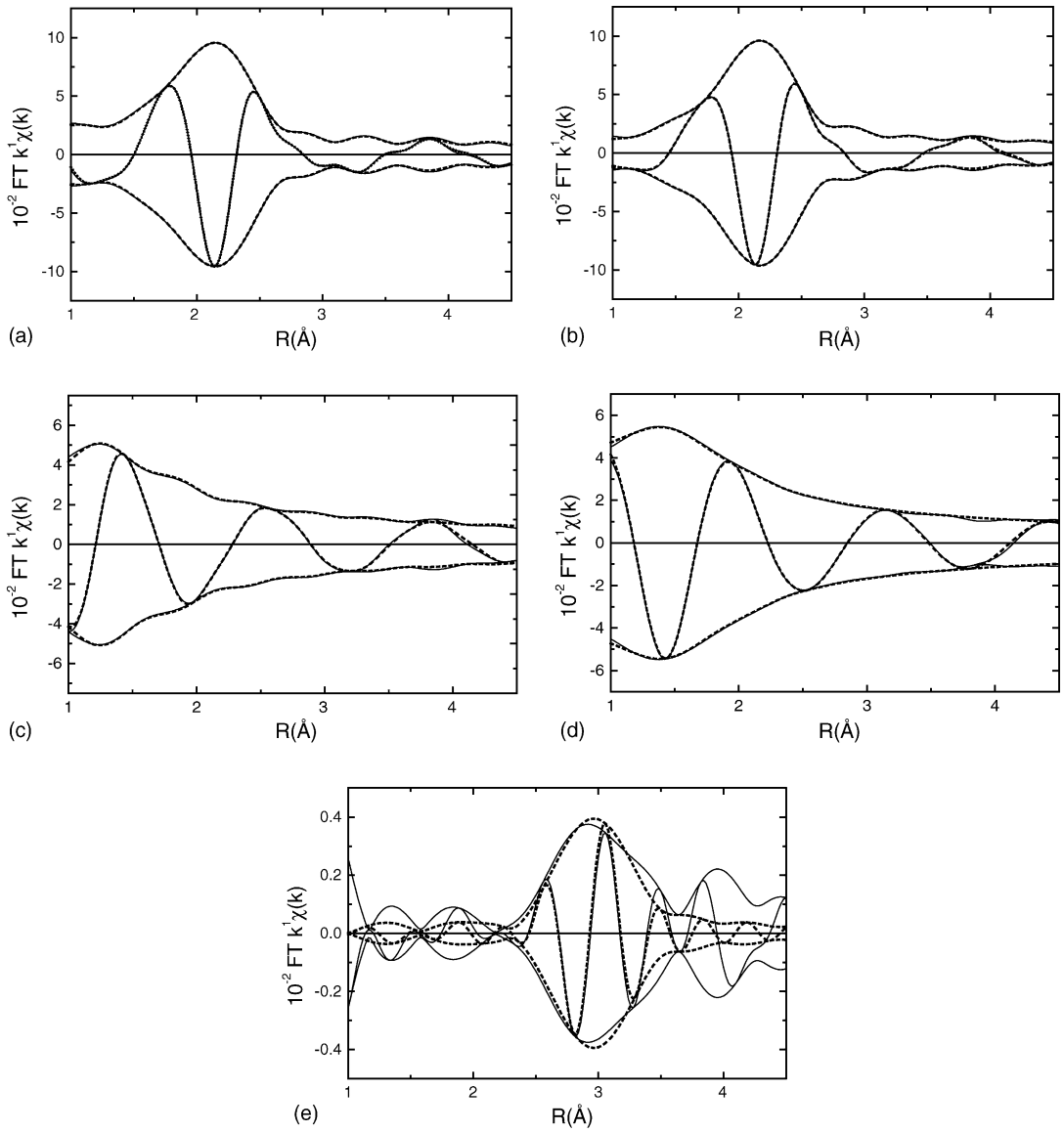

Fig. 3. (a) Fourier transforms (k^1, Δk = 2.5–9 Å^{-1}) of the raw data (—) and fit (- - -) of the hydrogenated Mg_2Ni film and difference files Fourier transforms in k^1 of the raw data (—) and fit (- - -) of (b) Ni–Mg, (c) Ni–H, (d) Ni–H and (e) Ni–Ni.

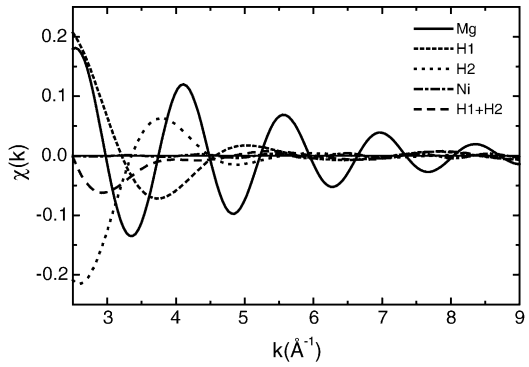

Fig. 4. Calculated $\chi(k)$ of the different atomic contributions to the total fit for the hydrogenated Mg_2Ni film.

of the noise. It is also possible that this feature influences the quality of the Ni–Ni fit slightly.

The calculated individual EXAFS contributions from the analysis of the hydrogenated film are shown together in Fig. 4. The presence of the Ni–Mg contribution (solid line) is dominant in a large part of k space. The two Ni–H shells are out of phase at high values of k, as is clear from the opposite signs of the amplitude. However, the sum of the hydrogen shells clearly shows a significant hydrogen presence (dashed line) at low values of k ($k < 5$ Å^{-1}). The Ni–Ni contribution is not visible in this plot due to the scale used.

The sum of the FT of the two Ni–H shells of the hydrogenated film are shown in Fig. 5a together with the fit. Comparing the shape of the amplitude of the FT with the FT amplitude of the Ni–H contribution in the virgin film in Fig. 5b, we note a distinct difference. The different signature of both plots shows that hydrogen is indeed present in different configurations in the virgin and hydrogenated films. This demonstrates the power of the difference file technique, as an integral part of the XDAP program, which allows us to resolve such multiple shells in the EXAFS data.

In Table 3 the strong decrease of the first shell magnesium coordination upon hydrogenation is clear. Only one Ni–Mg contribution can be detected at a distance of 2.63 Å. This distance is slightly shorter than that of the first magnesium shell in the virgin film (Table 2). A considerable increase of the total Ni–H coordination is found. In contrast to the virgin film, two hydrogen shells are detected in the hydrogenated film. A new Ni–H shell with a coordination of 4.4 appears at 1.57 Å. The hydrogen shell at 1.86 Å, close to the value of 1.85 Å for the virgin film, has a coordination of 16. The

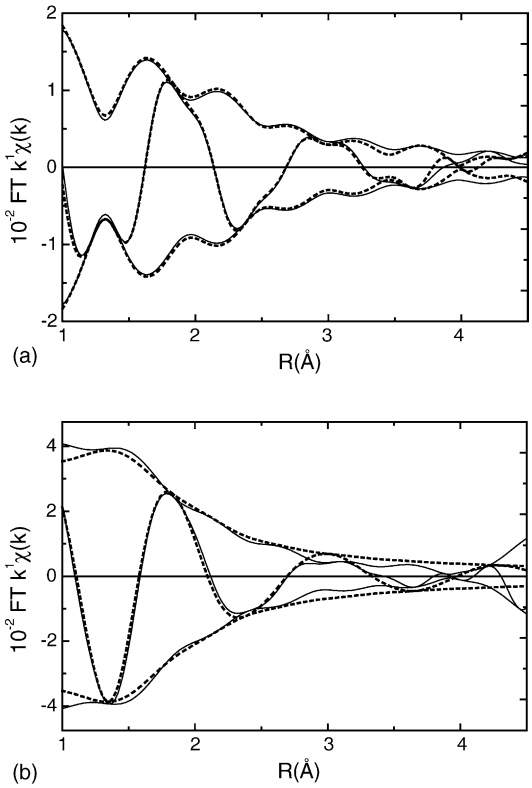

Fig. 5. Fourier transforms (k^1, $\Delta k = 2.5$–9 Å^{-1}) of the raw data (—) and fit (- - -) of the difference files Fourier transforms in k^1 of (a) the sum of both Ni–H contributions in the hydrogenated film and (b) the single Ni–H contribution in the as-deposited film.

difference in the Debye–Waller factors ($\Delta\sigma^2$) is striking; the hydrogen shell at 1.85 Å has a value three times larger than that of the hydrogen shell at 1.57 Å. As in the virgin film, a very small number of nickel neighbours is detected in the hydrogenated film, as indicated by the coordination of 0.2. The Ni–Ni Debye–Waller factor is very low, probably the result of the neighbouring feature in the FT, which tends to broaden the fit.

Table 4 shows the fit parameters of the Mg_2Ni film after a heat treatment, which removes hydrogen from the film. As in the virgin film two Ni–Mg contributions at different distances are found. The coordination of the first magnesium shell has increased slightly although it remains close to the value of the hydrogenated film. The same is true for the Ni–Mg distance, which has also increased slightly and remains close to the previous values. The second Ni–Mg contribution is, like the

Table 3
Ni K-edge; sample Mg_2Ni/Pd hydrogenated; EXAFS analysis (2.5 Å^{-1} < k < 9 Å^{-1}) k^1-weighing

Absorber–backscatterer	N	R (Å)	$\Delta\sigma^2$ (10^{-3} Å^2)	ΔE_0 (eV)	k variance	
					Imaginary	Real
Ni–Mg	2.7	2.63	7.6	−4.1	0.05	0.01
Ni–H	4.4	1.57	7.9	7.0		
Ni–H	16.0	1.86	25	14.1		
Ni–Ni	0.2	3.38	0.8	4.3		

Table 4
Ni K-edge; sample Mg_2Ni/Pd dehydrogenated; EXAFS analysis ($2.5\,Å^{-1} < k < 8\,Å^{-1}$) k^1–weighing

Absorber–backscatterer	N	R (Å)	$\Delta\sigma^2$ (10^{-3} Å^2)	ΔE_0 (eV)	k variance	
					Imaginary	Real
Ni–Mg	3.1	2.69	13	−8.6	0.14	0.05
Ni–H	3.2	1.77	7.2	10.8		
Ni–Mg	2.7	4.09	38	−11.8		

second Ni–Mg contribution in the virgin film, at a large distance from the nickel atom (4.1 Å). Hydrogen is still present in the film as is clear from the coordination of 3.4 at a distance of 1.8 Å. This amount is, however, less than half of the hydrogen content of the virgin film at the same Ni–H distance. A nickel contribution was not required to fit the EXAFS data satisfactorily.

The number of independent parameters (N_{ind}), which is allowed for the fit procedure of the EXAFS data [21] is 17 for the virgin and hydrogenated samples is 17 and 14 for the dehydrogenated film. The numbers of free fit parameters for the fits are 16 for the virgin and hydrogenated film and 12 for the dehydrogenated sample. Mathematically, this means that the EXAFS data is not over-fitted.

Fig. 6 shows the X-ray diffraction spectra of the film, as-deposited, and after exposure to 950 mbar H_2. The latter spectrum has been shifted along the y-axis for clarity. In the metallic state (a) two reflections are observed corresponding to the (0 0 3) and (0 0 6) lattice planes of the hexagonal lattice of Mg_2Ni. The absence of further reflections, points to a textured growth of the films with the c-axis out-of-plane, although rocking scans reveal a full width at half maximum of several degrees. From the peak width in the growth direction the grain size is estimated to be 30 nm; the crystallinity is poor. Exposure to a hydrogen atmosphere yields a shift of the (0 0 3) and (0 0 6) reflections to smaller 2θ values, indicating a lattice expansion as hydrogen is incorporated in solid solution into the lattice. As more hydrogen is introduced, the intensity of the crystal reflection decreases but no reflections corresponding either to LT Mg_2NiH_4 or HT Mg_2NiH_4 appear. The evolving phase is XRD amorphous (see Fig. 6b; the broad peak at around $2\theta = 19^\circ$ is a background peak due to the loading cell). Unloading at 100 °C restores crystalline order of Mg_2Ni; however, the increased peak width and smaller intensity indicate that the crystallinity is reduced with respect to that of the virgin film.

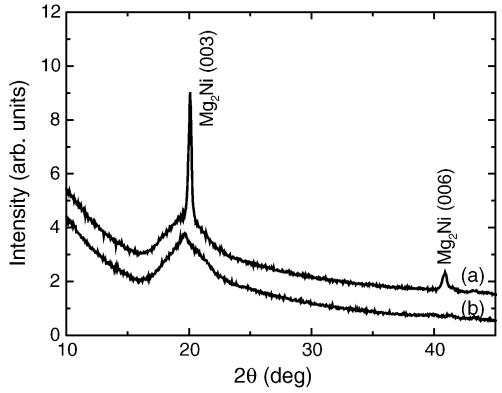

Fig. 6. X-ray scans of 200 nm Mg_2Ni/3 nm Pd: (a) as deposited and (b) in 950 mbar H_2. For clarity the latter spectrum has been shifted along the y-axis. Upon exposure to hydrogen the monocrystalline Mg_2Ni vanished; no long-range order in Mg_2NiH_4 could be detected.

4. Discussion

4.1. Absorption edges

The absorption edge of an XAFS spectrum provides information about the electronic state of the probed atom. The nickel edge shifts from 2.7 eV to higher energy upon hydrogenation. This is in good agreement with the value of 2.5 eV, reported by Richardson et al. [22] and confirms complete loading of our Mg_2Ni film. The edge shift is the result of charge transfer between the nickel atom and its surroundings.

Farangis et al. [12] have shown that the nickel L_2 and L_3 absorption edges and the magnesium K-edge shift to lower energy with increasing nickel content. The magnesium K-edge shift is explained by a reduced coordination around magnesium. The absorption edge shift of nickel indicates that in the NiMg alloy the electrons tend to be located at the nickel atom. Hydrogenation of the alloy produces a structure in which hydrogen is covalently bonded to nickel in a $[NiH_4]^{4-}$ complex [23,24]. Magnesium donates its valence electrons to the $[NiH_4]^{4-}$ complex. Although nickel is part of a negatively charged complex, the absorption edge shift to higher energy indicates an electron transfer. Since in this complex the donated electrons of the magnesium atoms are located at the hydrogen atoms instead of on the nickel atom as in the alloy, less charge is found on the nickel atom explaining the direction of the edge shift.

The heat treatment resulting in dehydrogenation causes the absorption edge to shift back to its original position. This confirms complete unloading of the film.

4.2. The metal structure

The EXAFS analysis of the virgin film provides information on the nearest neighbours of nickel as shown in Table 2.

Magnesium has the largest contribution in the EXAFS spectrum. The first shell Ni–Mg distance of 2.67 Å is close to the literature value for Mg_2Ni [7]. This is also confirmed by the XRD result, which shows that the detected *c*-axis lattice parameter $c = 13.25$ Å is close to the $c = 13.20$ Å reported for Mg_2Ni [7]. The slightly higher value might be an indication that the as-deposited film already contains some hydrogen. However, the Ni–Mg coordination of 5.3 is much smaller than the expected value of 8. This means that the as-deposited film does not have a homogeneous structure. The XRD results show that at least a part of the film is nanocrystalline Mg_2Ni. Based on the coordination numbers, we estimate that about two-third of the film is in the Mg_2Ni crystalline structure. The rest of the film is very likely amorphous Mg_2Ni. Farangis et al. [12] did not detect nickel-nearest neighbours around magnesium in their Mg_2Ni thin film; their film was probably completely amorphous.

With the XAFS techniques, hydrogen has recently been detected [25] as a scattering neighbour atom in covalent bonding in water. Hydrogen has also been detected indirectly by Pd–Pd lattice expansion using the lens effect in hydrides [26]. In a study of the gadolinium–magnesium switchable mirror, Di Vece et al. [13], showed that hydrogen can also be directly detected in a metal. The coordination of 7.3 found here shows that hydrogen is absorbed during deposition of the Mg_2Ni film. The Ni–H distance is 1.86 Å, much larger than the value of 1.57 Å, expected for the Mg_2NiH_4 structure. Moreover, a hydrogen coordination of 7.3 is much too large for a first shell; this would imply that the film is completely loaded. We know that this is not the case; we, therefore, conclude that more hydrogen is detected than would be plausible based on the presence of a NiH_4 complex. The explanation for this large hydrogen coordination is that the detected hydrogen originates from a second and/or third hydrogen shell, which can have a large number of contributing atoms. This is schematically illustrated in Fig. 7. It shows that this is possible when the hydrogen constituting this second and/or third shell is bonded to a nearest neighbour nickel atom.

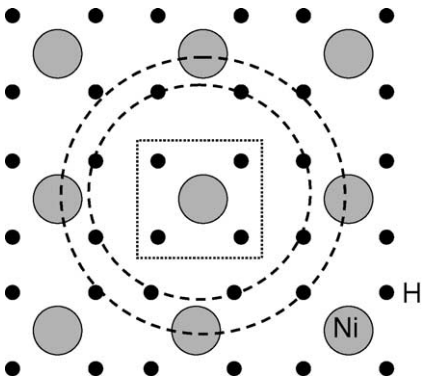

Fig. 7. Schematic illustration of multiple hydrogen shells around a NiH_4 complex.

The second-shell hydrogen coordination of 7.3 suggests a large hydrogen content in the virgin film. However, a detected hydrogen atom in the second-shell is shared by all of its nickel second-nearest neighbours; it is, therefore, 'over-counted'. To obtain the actual Ni/H ratio, the second-shell coordination number has to be divided by the number of nearest-neighbour nickel atoms to the hydrogen atom. The nickel coordination number around a hydrogen atom is not known but likely has a value of around 10. This then gives 0.7 hydrogen atoms in the second hydrogen shell around a nickel atom. Since we know from XRD and isotherms of Mg_2NiH_4 that the amount of hydrogen in the virgin film is less than 10% [27], it is realistic to assume that there are at least 10 second-nearest-neighbour hydrogen positions which can be occupied or not. An occupancy of the available hydrogen positions of less than 10% would result in less than 0.4 hydrogen atoms as a first-nearest-neighbour shell. The noise in the EXAFS spectrum masks this contribution preventing detection.

The detection of a large number of magnesium second-nearest neighbours at a distance of 4.5 Å is a strong evidence for long-range order in part of the film. The low Ni–Ni coordination at a distance of 3.5 Å indicates that nickel clusters with an ordered structure are not present in the film. Their disorder prevents detection from the EXAFS data.

4.3. The metal hydride structure

From Table 3 it is clear that the Ni–Mg coordination has decreased upon complete hydrogenation. The Ni–Mg coordination should be eight [23,24]; our much smaller value indicates that the hydrogenated film does not have a well-defined structure. The Ni–Mg distance decreases slightly to 2.63 Å. From the absorption edge shift we know that the film is almost completely loaded with hydrogen. This excludes the possibility that part of the film remains in the unloaded Mg_2Ni state. The reduction of the number of magnesium nearest neighbours can have two causes: (1) the decreasing size of the nanocrystallites leaving a higher surface/bulk ratio; (2) an increase of the amorphous fraction of the film, with less well-defined Ni–Mg distances.

According to Soubeyroux et al. [28] the LT phase of Mg_2NiH_4 has an average Ni–Mg distance of 2.64 Å. This is close to our measured value of 2.63 Å. Since the film is XRD-amorphous, an LT Mg_2NiH_4 structure could only be part of nanocrystallites. The Ni–Ni contribution at a distance of 3.4 Å is, however, not in agreement with the LT structure. From the decreasing Ni–Ni coordination, we also know that phase segregation does not occur. This would lead to nickel nanocluster formation, e.g., an increase of the Ni–Ni coordination. The low Ni–Ni coordination is explained by a large degree of disorder.

The results of Table 3 also indicate the presence of two hydrogen shells. Upon hydrogenation the shell at 1.86 Å clearly shows a large increase in coordination. A new shell appears at 1.57 Å, a distance similar to that in LT Mg_2NiH_4. The coordination of 4.4 in this shell confirms complete loading of

the film, as expected for the $[NiH_4]^{4-}$ complex in Mg_2NiH_4. If the coordination of hydrogen at a distance of 1.57 Å is that needed for complete loading, the hydrogen at a distance of 1.86 Å must belong to another atom. The sum of the Ni–H distances of the two hydrogen shells, gives the Ni–Ni distance as reported in Table 3. This suggests that the hydrogen atom in this second shell is not bonded to a magnesium atom but to the nearest-neighbour nickel atom. Therefore, the hydrogen at this distance is again identified as second nearest-neighbour, attached to the nearest-neighbour nickel atoms. The Ni–Ni and Ni–H distances do not agree with the LT structure of Mg_2NiH_4. In this structure the second hydrogen shell should also be located at a much larger distance. This means that the structure of Mg_2NiH_4 in a thin film is completely different from that reported for the bulk alloy.

The much higher Debye–Waller factor for the second hydrogen shell as compared to the first shell is the result of a large disorder of the nickel atoms to which hydrogen is bonded. The difference in the amount of disorder between the first and second hydrogen shell causes the effect in which the relative increase of the hydrogen coordination in the two hydrogen shells differs. Due to large disorder the coordination of hydrogen positioned at about 1.86 Å increases by about a factor of only two since much of the hydrogen is not detected. The coordination number of hydrogen positioned at 1.57 Å increases by much more (from less than 0.4–4.4). The high order of hydrogen in this first shell allows detection of all of the hydrogen in this fully loaded first shell. The marked increase of the total Ni–H coordination confirms the complete loading of the film with hydrogen.

4.4. The dehydrogenated structure

As seen in Table 4 the Ni–Mg coordination at about 2.7 Å increases slightly upon dehydrogenation. This indicates that the structurally well-ordered fraction of the film is constant. The Ni–Mg distance increases again to a value close to that of the virgin film. It is, therefore, likely that part of the original structure is restored. This is probably caused by the thermal treatment of 100 °C.

The reappearance of a second magnesium shell is probably the result of the contraction of the interatomic distance upon dehydrogenation. The slight order in this second magnesium shell again enters the range of detection.

The strong decrease of the Ni–H coordination at 1.8 Å and the absence of the hydrogen shell at 1.5 Å confirm dehydrogenation. Clearly, a residue of hydrogen remains after dehydrogenation, probably in magnesium-rich parts of the film. Since it is known that Mg_2Ni films remain optically switchable after dehydrogenation, we conclude that a well-ordered structure is not necessary to explain the optical transparency in the hydrogenated state. Besides a structural interpretation of the properties of the film, future research should focus on an explanation, based on the amorphous or nanocluster nature of a switchable mirror.

5. Conclusions

From the EXAFS analysis, we conclude that the as-deposited film is already in a structurally mixed state. The film contains both nanocrystalline and amorphous regions. Hydrogenation results in a decrease of order; the film becomes completely amorphous. However, four hydrogen atoms are found around a nickel atom, confirming the formation of a $[NiH_4]^{4-}$ complex. Besides the observed absorption edge shift, a large increase of the hydrogen coordination upon hydrogenation confirms loading of the film. Oxygen could not be detected in the virgin, loaded and deloaded films. A change in lattice parameters upon dehydrogenation of the film indicates a slight partial recovery of the crystalline Mg_2Ni structure. However, the structure of the major part of the film remains disordered. Models to explain the optical properties of Mg_2Ni switchable mirrors should focus on a system that is more disordered than previously considered.

References

[1] R. Griessen, Europhys. News 32 (2) (2001) 42.
[2] J.N. Huiberts, R. Griessen, J.H. Rector, R.J. Wijngaarden, J.P. Dekker, D.G. de Groot, N.J. Koeman, Nature 380 (1996) 231.
[3] P. van der Sluis, M. Ouwerkerk, P.A. Duine, Appl. Phys. Lett. 70 (1997) 3356.
[4] P. van der Sluis, V.M.M. Mercier, Electrochim. Acta 46 (2001) 2167.
[5] T.J. Richardson, J.L. Slack, R.D. Armitage, R. Kostecki, B. Farangis, M.D. Rubin, Appl. Phys. Lett. 78 (2001) 3047.
[6] A. Reiser, B. Bogdanović, K. Schlichte, Int. J. Hydrogen Energy 25 (2000) 425.
[7] J. Schefer, P. Fischer, W. Hälg, F. Stucki, L. Schlapbach, J.J. Didisheim, K. Yvon, A.F. Andresen, J. Less-Common Met. 74 (1980) 65.
[8] J. Isidorsson, I.A.M.E. Giebels, R. Griessen, M. Di Vece, Appl. Phys. Lett. 80 (2002) 2305.
[9] P. Zolliker, K. Yvon, Mater. Res. Bull. 21 (1986) 415.
[10] G.N. Garcia, J.P. Abriata, J.O. Sofo, Phys. Rev. B 59 (1999) 11746.
[11] W.R. Myers, L.-W. Wang, T.J. Richardson, M.D. Rubin, J. Appl. Phys. 91 (2002) 4879.
[12] B. Farangis, P. Nachimuthu, T.J. Richardson, J.L. Slack, R.C.C. Perera, E.M. Gullikson, D.W. Lindle, M. Rubin, Phys. Rev. B 67 (2003) 085106.
[13] M. Di Vece, A.M.J. van der Eerden, J.A. van Bokhoven, S. Lemaux, J.J. Kelly, D.C. Koningsberger, Phys. Rev. B 67 (2003) 035430.
[14] F.W. Kampers, T.M.J. Maas, J. van Grondelle, P. Brinkgreve, D.C. Koningsberger, Rev. Sci. Instrum. 60 (1989) 2645.
[15] G. Derbyshire, K. Cheung, P. Sangsingkeow, S. Hasnain, J. Synchr. Rad. 6 (1999) 62.
[16] M. Vaarkamp, J.C. Linders, D.C. Koningsberger, Physica B 208 (1995) 159.
[17] B.K. Teo, EXAFS: Basic Principles and Data Analysis, Springer, New York, 1986.
[18] J.W. Cook Jr., D.E. Sayers, J. Appl. Phys. 52 (1981) 5024.
[19] J.J. Rehr, R.C. Albers, Rev. Mod. Phys. 72 (2000) 621.
[20] A.L. Ankudinov, B. Ravel, J.J. Rehr, S.D. Conradson, Phys. Rev. B 58 (1998) 7565.
[21] D.C. Koningsberger, B.L. Mojet, G.E. van Dorssen, D.E. Ramaker, Top. Catal. 10 (2000) 143.

[22] T.J. Richardson, B. Farangis, J.L. Slack, P. Nachimuthu, R. Perera, N. Tamura, M. Rubin, J. Alloys Compd. 356/357 (2003) 204.
[23] K. Yvon, J. Less-Common Met. 103 (1984) 53.
[24] M. Gupta, L. Schlapbach, Topics in Applied Physics, Hydrogen in Intermetallic Compounds I, 63, Springer, Berlin, 1988, 139.
[25] K.R. Wilson, J.G. Tobin, A.L. Ankudinov, J.J. Rehr, R.J. Saykally, Phys. Rev. Lett. 85 (2000) 4289.
[26] B. Lengeler, Phys. Rev. Lett. 53 (1984) 74.
[27] W. Lohstroh, R.J. Westerwaal, J.L.M. van Mechelen, C. Chacon, E. Johansson, B. Dam, R. Griessen, Phys. Rev. B 70 (2004) 165411.
[28] J.L. Soubeyroux, D. Fruchart, A. Mikou, M. Pezat, B. Darriet, Mater. Res. Bull. 19 (1984) 895.